

Remote Triggering of Microearthquakes and Tremor in New Zealand following the 2016 $M_{\rm w}$ 7.8 Kaikōura Earthquake

by Zhigang Peng, Bill Fry, Kevin Chao, Dongdong Yao, Xiaofeng Meng, and Art Jolly

Abstract We conduct a systematic search for remotely triggered seismicity in New Zealand following the 2016 $M_{\rm w}$ 7.8 Kaikōura earthquake. We first examine seismicity rates obtained from the GeoNet catalog one month before and after the Kaikōura mainshock. We find a clear increase of microseismicity following the mainshock in the North Island, mostly along the shallow portion of the Hikurangi subduction zone, as well as surrounding and to the east of the Taupo volcanic zone (TVZ). We then examine high-frequency seismic signals during and immediately following the large-amplitude surface waves and identify instantaneously triggered events at several new sites. These include long-duration tremor-like signals in low-strainrate regions around Auckland, near the source region of the 2009 $M_{\rm w}$ 7.9 Dusky Sound earthquake in the southern South Island and at several sites within and south of the TVZ. Triggered signals along the TVZ likely originated from multiple sources. A common feature of these instantaneous triggering sites is their close proximity to hot springs or elevated subsurface temperatures associated with active volcanoes or fault structures, suggesting that they may provide necessary conditions for remote dynamic triggering.

Electronic Supplement: Table of location parameters for triggered sources and waveform plots showing evidence of triggered tremor, best-fitting location for the high-frequency tremor bursts, \log_{10} 10 Hz envelopes, and raw and 5-Hz high-pass-filtered vertical-component seismograms.

Introduction

Large earthquakes are known to trigger shallow microearthquakes or deep tectonic tremor at long-range distances (e.g., $\sim 10^2$ to $\sim 10^4$ km), a phenomenon generally known as remote dynamic triggering (e.g., Peng and Gomberg, 2010; Hill and Prejean, 2015). The term "dynamic" refers to the fact that at such distances (typically hundreds to thousands of kilometers away from the earthquake source), the static stress change from permanent fault displacements of large mainshocks is negligible compared with the local stress regime at the triggered location, and dynamic stress from passing seismic waves is the most likely agent to trigger microseismicity (Brodsky and van der Elst, 2014; Hill and Prejean, 2015) and other aseismic and hydrological processes (Wang and Manga, 2010; Manga et al., 2012; Cox et al., 2015). Because dynamic triggering mostly occurs in places that are critically stressed and close to failure (Brodsky and van der Elst, 2014), an improved understanding of dynamic triggering not only elucidates earthquake interactions at regional and global scales (e.g., Michael, 2011; Pollitz et al., 2012) but also illuminates how the local stress state evolves from subcritical to failure.

Hence, dynamically triggered events provide a unique window into the process of earthquake nucleation (e.g., Gonzalez-Huizar and Velasco, 2011; Hill, 2012; Tape *et al.*, 2013; Brodsky and van der Elst, 2014; Han *et al.*, 2017) and stress relaxation processes (e.g., Brodsky, 2006; Opris *et al.*, 2017).

In this study, we conduct a systematic search for remotely triggered seismicity (microearthquakes and tremor) following the 2016 $M_{\rm w}$ 7.8 Kaikōura earthquake (Fig. 1). This event ruptured many fault segments along the complicated Marlborough fault system in the South Island (Hamling *et al.*, 2017; Kaiser *et al.*, 2017; Nicol *et al.*, 2018; Wen *et al.*, 2018). It was the second largest seismic event since European settlement in New Zealand after the 1855 $M_{\rm w} \sim 8.2$ Wairarapa earthquake and was followed by triggered slow-slip events along the Hikurangi subduction zone (HSZ; Wallace *et al.*, 2017). Here, we examine earthquake catalogs and waveforms recorded by GeoNet to identify regions that show clear evidence of dynamic triggering following the mainshock. We first describe the available data and our analysis procedure. Next, we present evidence of triggered seismicity inferred from

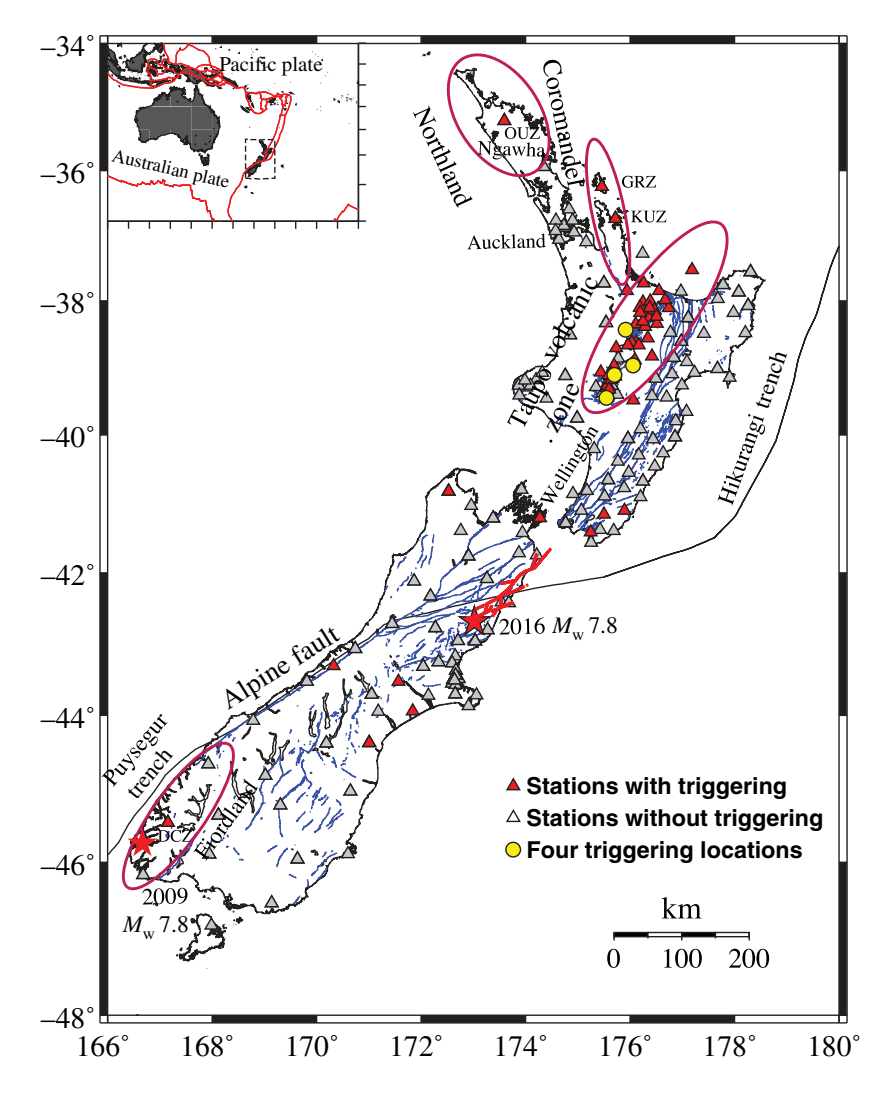


Figure 1. Map of the study region in New Zealand. The star marks the epicenter of the $2016\,M_{\rm w}$ 7.8 Kaikōura mainshock, and thick lines nearby mark its surface ruptures (Hamling *et al.*, 2017). Thin lines mark other active faults. Seismic stations with clear and no evidence of dynamic triggering are marked by triangles with different shadings, respectively. Four circles around the Taupo volcanic zone (TVZ) in the North Island mark the epicentral locations of four sites with clear evidence of triggered seismicity during the mainshock surface waves (Fig. 8). Ovals mark selected regions with relatively high subsurface temperatures (Reyes *et al.*, 2010). The inset marks the study region in a larger tectonic context of southern Pacific. The color version of this figure is available only in the electronic edition.

earthquake rate and waveform analyses. Finally, we discuss the significance of the triggering sites and implications on dynamic triggering mechanisms.

Data and Analysis Procedure

The analysis procedure includes two parts. First, we examine seismicity rate changes outside of the immediate aftershock zone before and after the $M_{\rm w}$ 7.8 Kaikōura mainshock using earthquakes around New Zealand listed in the GeoNet catalog (longitudes between 166° and 180° E and latitudes between 34° and 48° S). We quantify rates of events in the catalog for one month before and after the Kaikōura earthquake.

Next, we compute the magnitude of completeness M_c for the entire catalog using a maximum curvature (MAXC) method (Wiemer and Wyss, 2000; Wiemer, 2001). We use the M_c determined by the MAXC method + 0.2 as the threshold, because Woessner and Wiemer (2005) found that this method resulted an underestimate of the $M_{\rm c}$ compared with other methods. Because many early aftershocks of the $M_{\rm w}$ 7.8 mainshock were missing in the catalog (Chamberlain et al., 2017), this could result in higher M_c values than at other times. We also spatially and temporally divide the region into North and South Islands, and before and after the mainshock, to compute the M_c value separately. Finally, we discretize the entire region into grid cells of 0.25° by 0.25° and compute the β -statistics for earthquakes with magnitudes above the $M_{\rm c}$ value (Aron and Hardebeck, 2009). The β -value is defined as

$$\beta = \frac{N_a - N(T_a/T)}{\sqrt{N(T_a/T)(1 - (T_a/T))}},$$
 (1)

in which T_a is the time length of the triggering window after the mainshock, T is the entire time window (i.e., the time length of the background seismicity window plus the triggering window), and N_a and N are the number of events detected in T_a and T, respectively. This metric is commonly used to identify regions exhibiting seismicity rate changes after a mainshock (e.g., Gomberg *et al.*, 2004; Meng and Peng, 2016; Li *et al.*, 2017). As in previous studies, regions with β -values larger than 2 or less than -2 are considered to have statistically significant increases or decreases following the mainshock (Hill and Prejean, 2015).

The second part of our study involves detailed waveform analysis to identify

remotely triggered tremor and microearthquakes during and immediately following the $M_{\rm w}$ 7.8 mainshock. We first download 3 hrs of continuous waveforms (1 hr before and 2 hrs after the mainshock) recorded by broadband and short-period stations operated by the GeoNet. Next, we apply a 10-Hz high-pass filter to the vertical-component data and visually examine the recorded high-frequency ground motion during and immediately following the mainshock. This frequency range is similar to those used in detecting remotely triggered tremor at similar distance ranges (Guilhem *et al.*, 2010; Aiken *et al.*, 2015; Peng *et al.*, 2015). We identify triggered tremor as long-duration (10–20 s) signals without clear

P and S arrivals and with relatively symmetric waveforms during large-amplitude surface waves and triggered earthquakes as relatively short-duration (e.g., < 10 s) signals with clear P/S arrivals and asymmetric waveforms (i.e., abrupt onset and extended coda) during and immediately following the surface waves (Aiken et al., 2015). To rule out the possibility of false identification, we also visually inspect the raw data, its spectrogram (Peng et al., 2011), and the horizontal components to ensure that the original data were not clipped in any of the three components, which could result in spurious high-frequency signals in other components. Finally, if there are additional stations within 50 km, we also check their waveforms to search for similar high-frequency signals. If the tremor signal is present across multiple and proximal stations, we attempt to locate the source by time-shifting envelope functions and grid searching over a 3D volume (Chao et al., 2017).

Results

The Gutenberg-Richter frequencysize statistics for various space-time windows and the determination of M_c values are shown in Figure 2. Figure 3 shows one month of seismicity before and after the mainshock, as well as the β -value map with $M_c = 2.74$. The seismicity rate increases around the aftershock zone of the Kaikōura earthquake and in many regions in the North Island are obvious, especially in the central Taupo volcanic zone (TVZ) and several regions near the HSZ near the east coast. From the crosssection plot (Fig. 4), we find that the increase of seismicity off the coast of southern Hawke's Bay is likely associated with the subduction zone (cross section BB'). On the other hand, seismicity following the mainshock mostly occurred along crustal faults above the plate interface (cross sections AA', BB', and CC'). The seismicity increase in these regions likely occurred immediately following the mainshock (Fig. 5a). However, the increase off the coast of southern Hawke's Bay was not clear when comparing the 30-day background with 1-day seismicity following the mainshock (Fig. 5b). In addition, several regions show apparent reductions in seismicity rates following the

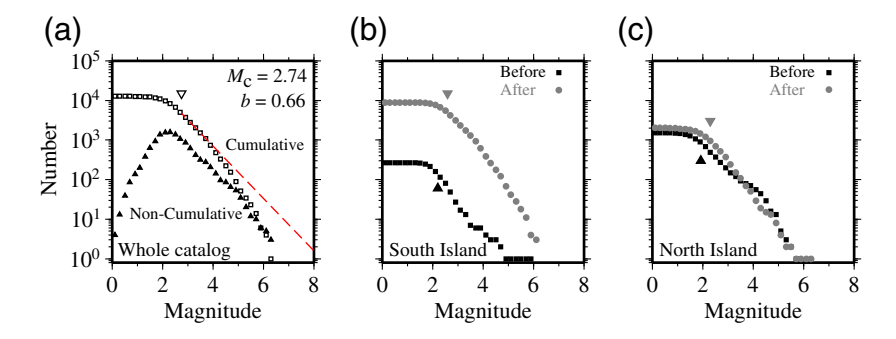


Figure 2. (a) Gutenberg–Richter (G-R) relationship for all seismicity within two months of the Kaikōura mainshock. The inverted triangle marks the M_c value as determined by the maximum curvature method + 0.2 (Wiemer, 2001). The dashed line marks the maximum-likelihood estimated b-value. (b) G-R relationship for seismicity in the South Island one month before and after the mainshock. (c) G-R relationship for seismicity in the North Island one month before and after the mainshock. The color version of this figure is available only in the electronic edition.

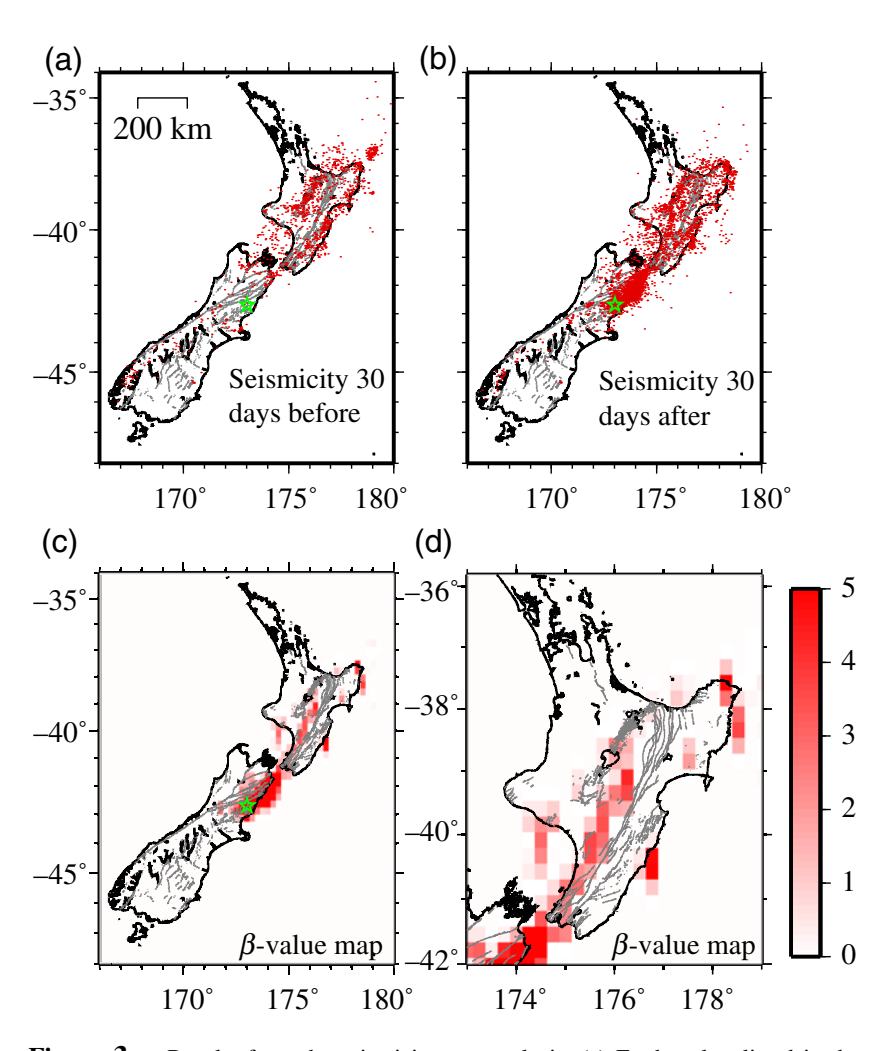


Figure 3. Results from the seismicity-rate analysis. (a) Earthquakes listed in the GeoNet catalog one month before the Kaikōura mainshock (star). (b) Earthquakes listed in the GeoNet catalog one month after the mainshock. (c) β -value map for the entire region with magnitude of completeness $M_c = 2.54$ and a grid spacing of 0.1°. (d) A zoom-in map to show the β -value map in the North Island. The color version of this figure is available only in the electronic edition.

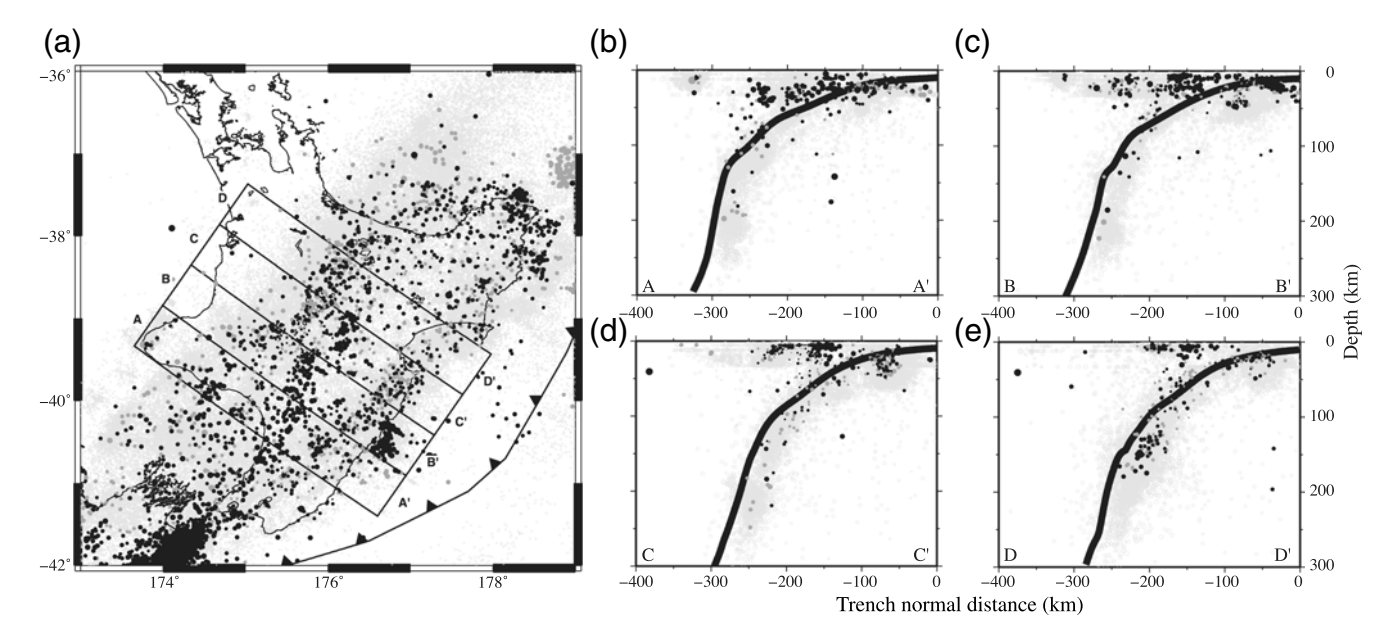


Figure 4. (a) Map in the North Island showing the seismicity one month before and after the Kaikōura mainshock. Seismicity in four cross sections is shown in (b)–(e). (b–e) Cross sections showing changes in seismicity following the mainshock. Solid lines mark the plate boundary model (Williams *et al.*, 2013).

mainshock. These include two spots within the TVZ and offshore near the epicentral region of an $M_{\rm w}$ 7.1 earthquake that occurred in September 2016 (Warren-Smith *et al.*, 2017). In comparison, the seismicity-rate changes are in isolated regions in the rest of South Island, including one region with an increasing rate on the northern Alpine fault.

With detailed waveform analysis, we find several regions with clear evidence of triggered tremor (Fig. 1), including four new regions where neither triggered nor ambient tremor has previously been reported. Figures 6 and 7 and (E) Figures S1 and S2 (available in the electronic supplement to this article) show detailed waveform plots for newly identified triggered tremor. In all these cases, clear highfrequency long-duration events occurred during transient stressing from passing large-amplitude surface waves. The first case is observed at Station OUZ at Omahuta, North of Auckland (Fig. 6). Rates of earthquakes in this region from the historical catalog are relatively low, with only three events with $M_{\rm w} > 3$ from 2006 to 2016 (within 100 km). The site is also over 200 km away from the plate boundary. Clear tremor-like signals were recorded only during the later cycles of the Rayleigh waves, although there were some hints of weaker high-frequency signals at the beginning of the Love-wave coda (Fig. 6c,d). The peak ground velocity values on the vertical and transverse components are 0.8 and 1.6 cm/s, which correspond to the peak dynamic stress of 80 and 160 kPa at the surface, respectively. This is calculated by assuming a nominal phase velocity of 3.5 km/s and a shear rigidity of 35 GPa (Fry et al., 2011; Hill and Prejean, 2015). Unfortunately, the next closest station (WCZ) is ~70 km away and did not record similar high-frequency signals. Because of this, we are unable to map the source region

of the tremor signals, but we note that it must lie close to Station OUZ.

The next group of triggered tremor is recorded at Stations GRZ (Great Barrier Island; Fig. 7) and KUZ (Kuaotunu; © Fig. S1) to the northeast and east of Auckland, the largest metropolitan center of New Zealand. As with the previous case at station OUZ, clear long-duration high-frequency signals occurred only during the peaks of large-amplitude surface waves. These stations are only ~60 km apart, and the recorded tremor signals have some similarities. However, with only two stations it is not clear whether they represent independent tremor sources or a common one.

The last case is only recorded at Station DCZ (Deep Cove) in Fiordland, South Island (E Fig. S2). There were two bursts of tremor-like signals during the large-amplitude surface waves, and a few of them were clipped on different components. Nevertheless, we verify that they are tremor-like signals, rather than earthquake-like or other artificially generated signals. Again, this is the only station in that region that has recorded these signals. We note that this station is ~ 100 km from the Puysegur trench.

The most abundant cases of triggering occurred along the TVZ, where several regions show evidence of triggered tremor and/or microearthquakes during and immediately following the large-amplitude surface waves (Fig. 8). We are able to identify at least four triggering sources. The first two are around Mt. Ruapehu and Mt. Tongariro, and the other two are near Lake Taupo and further north in the Rotorua region. The hypocentral depths of triggered seismicity determined from envelope cross correlations (by assuming them to be propagating *S* waves) are not well constrained. Around Mt. Ruapehu, only one very weak tremor-like signal was

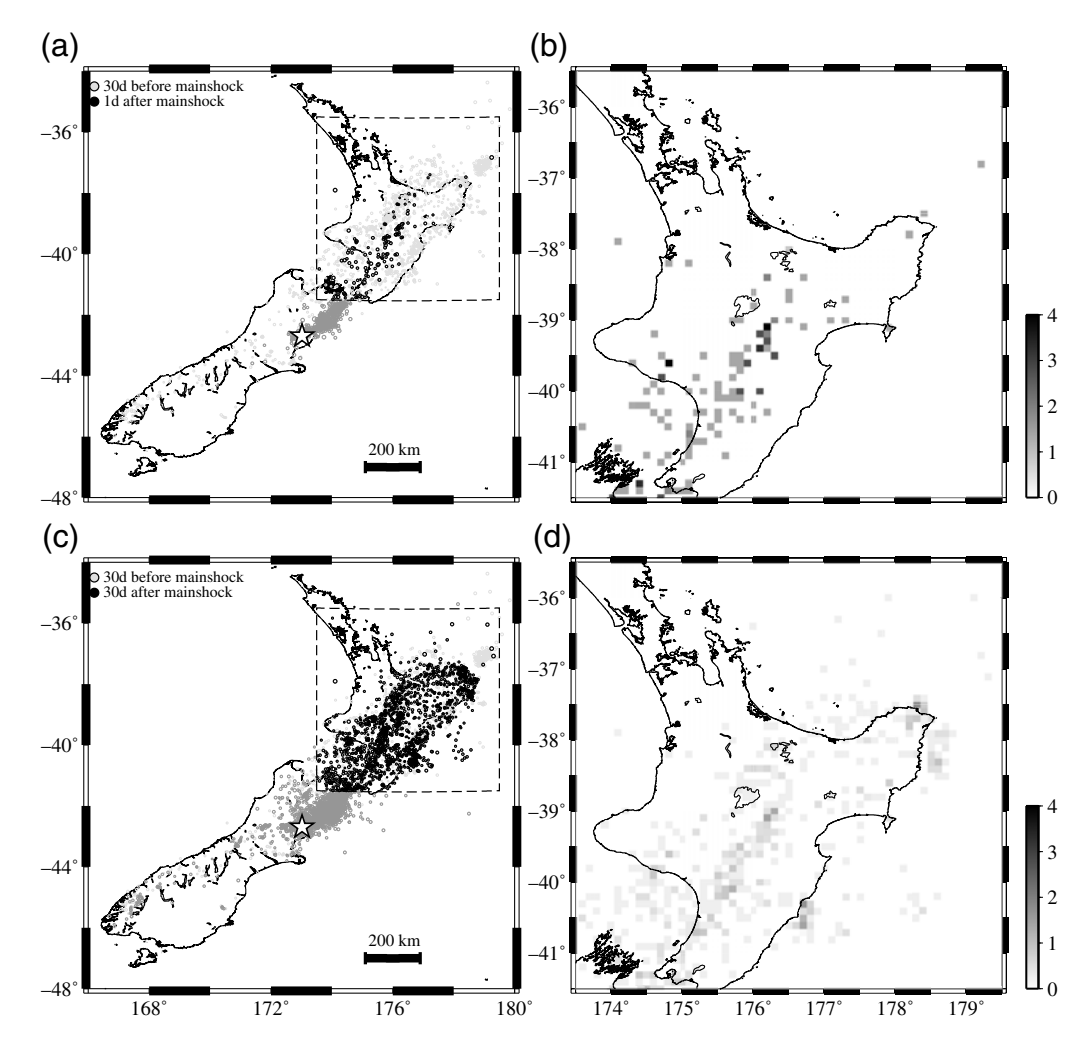


Figure 5. (a) Map showing the seismicity in the entire New Zealand one month before and one day after the Kaikōura mainshock. (b) The corresponding β -map in the North Island. (c) Same as (a) but with one month after the mainshock. (d) The corresponding β -map in the North Island.

recorded around 190–200 s after the mainshock (Fig. 8), and the hypocentral depth is 76 km (E Fig. S3). In Mt. Tongariro, the triggered seismicity occurred at a shallow depth of less than 10 km (E Figs. S5 and S6). The triggered events were at depths of 45–60 km in the rest two regions (E Figs. S6 and S7). We also note that many microearthquakes occurred immediately following those tremor events, and that most of them were not listed in the GeoNet catalog (E Fig. S8).

Discussions

In this study, we conducted a systematic search for remotely triggered seismicity (both regular microearthquakes and tremor) following the 2016 $M_{\rm w}$ 7.8 Kaikōura earthquake. We found clear increases in the rates of microseismicity in the North Island, mostly along the eastern coastline, as well as in some crustal faults along and to the east of the TVZ. This is consistent with the observation of shallow slow-slip events on

the subduction interface following the Kaikōura mainshock (Wallace et al., 2017), suggesting that microseismicity could be driven by the triggered slow-slip events. In addition, the fact that most triggered seismicity occurred in the North Island is compatible with large dynamic stressing from the directivity effect caused by the northward propagation of the mainshock rupture, resulting in higher ground motions (Bradley et al., 2017; Kaiser et al., 2017). Similar observations of preferential dynamic triggering in the rupture propagation direction were found following the 1992 $M_{\rm w}$ 7.2 Landers earthquake (Gomberg et al., 2001) and likely the 2002 $M_{\rm w}$ 7.9 Denali fault earthquake (Gomberg et al., 2004; Prejean et al., 2004). More recently, Enescu et al. (2016) and Miyazawa (2016) found similar evidence of triggered small- and moderate-size earthquakes at volcanoes and active faults in northeast Japan in the rupture propagation direction of the $M_{\rm w}$ 7.3 Kumamoto earthquake, consistent with the aforementioned directivity effects.

We note that static stress changes could be responsible for triggering earthquakes in the near field within a few fault

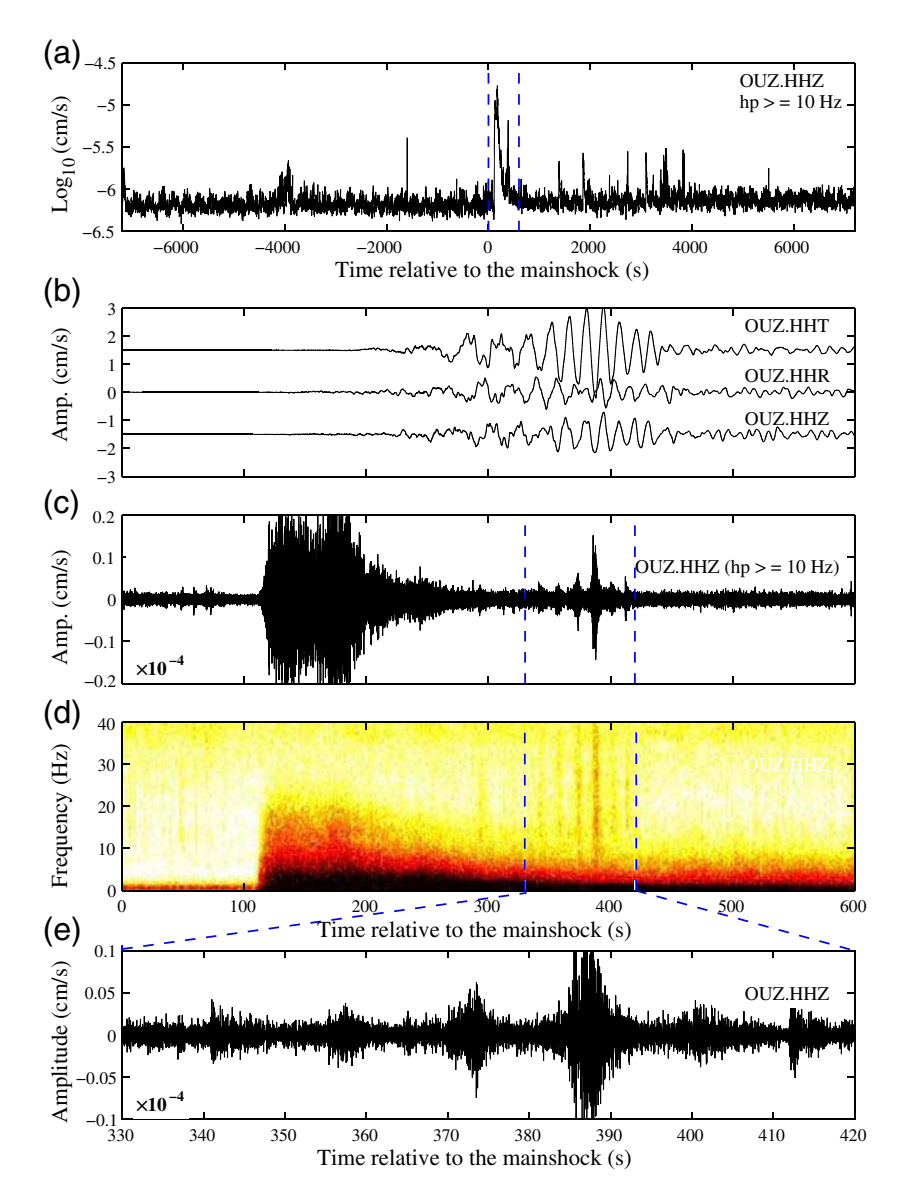


Figure 6. Waveform plots showing evidence of triggered tremor at Station OUZ (Omahuta). (a) Log_{10} 10-Hz high-pass-filtered envelope function 2 hrs before and after the Kaikōura mainshock. Vertical lines mark the time windows plotted in panels (b–d). (b) Instrument-corrected broadband signals recorded at station OUZ. (c) 10-Hz high-pass-filtered vertical-component seismogram showing the P wave of the mainshock and triggered tremor signals during the surface waves. (d) The corresponding spectrogram (i.e., frequency–time distribution), with stronger amplitudes marked by darker/warmer shadings. (e) A zoom-in plot showing the long-duration tremor-like signals. The color version of this figure is available only in the electronic edition.

lengths (King and Deves, 2015). However, except for the southernmost region of North Island, the static stress changes at the rest of the regions in the North Island were less than 2 KPa, whereas the dynamic stress changes are 1–2 orders higher (Wallace *et al.*, 2017). Hence, we conclude that the seismicity increase observed along the volcanic regions and elsewhere in the North Island are most likely caused by dynamic, rather than static stress changes.

We also found several new regions with possible triggered tremor sources. Among them, Station DCZ is within

50 km of the epicenter of the 2009 $M_{\rm w}$ 7.9 Dusky Sound megathrust earthquake (Fry et al., 2010). Hence, the likely source could be on or near the Puyseguer subduction zone. In this region, the most northern extent of the subduction zone meets the southern extent of the Alpine fault. Previously recorded tremor locations on the Alpine fault (Wech et al., 2012) are ~330 km from DCZ and are therefore not a likely source of the triggered tremor signal recorded at DCZ. This triggering source could also be related to mineral springs in Fiordland (Reyes et al., 2010) or originate from many cave systems in this region. Similar observations were made in Hokkaido, Japan, following the 2004 $M_{\rm w}$ 9.2 Sumatra earthquake (Obara, 2012), where triggered tremor was possibly associated with a limestone cave system, because there were no active faults nearby, and the subducting slab is too deep to effectively generate high-frequency tremor signals.

The remaining triggered tremor sources are in the North Island. Among them, tremor recorded at Stations OUZ, GRZ, and KUZ is not likely associated with the subduction zones, because the interface is at least a few hundred kilometers deep at these regions (Williams et al., 2013). From the online New Zealand Active Fault Database (see Data and Resources), no active faults were found near Station OUZ, and two normal faults are within 100 km of Stations GRZ and KUZ. Hence, these triggering signals may not be of tectonic origin. Station OUZ is located about 30 km from the Waiariki Pools, Ngawha Springs area in Northland, where fluid temperatures at surface are in the 40°C range. In addition, there are Miocene volcanic rocks in the area called the Kerikeri Volcanic Group from Kerikeri to Whangarei (Heming, 1980; Boodin et al., 2011). The Auckland volcanic field and volcanic island of Rangitoto

are all around the city of Auckland, and the extinct Coromandel volcanic zone and the associated hot springs (Reyes *et al.*, 2010; Boodin *et al.*, 2012) could be potential tremor-generating sources.

Most instantaneously triggered seismicity occurred along the TVZ (Fig. 8). However, the spatial patterns are complicated. Based on visual inspections, we identified at least four common sources with variable depths. However, because they did not completely account for all the observed triggering signals, it is very likely that additional sources were triggered. For stations near Mt. Tongariro, the high-frequency bursts

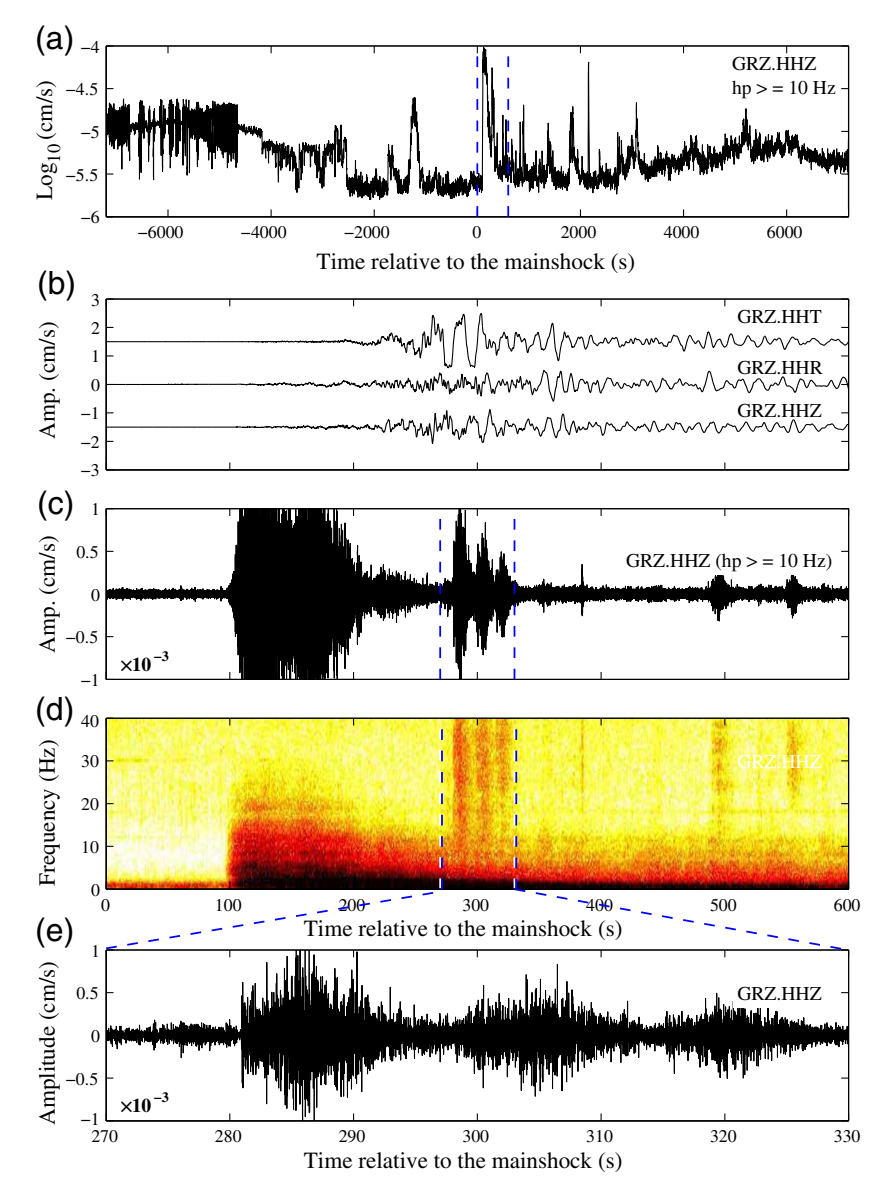


Figure 7. Waveform plots showing evidence of triggered tremor at Station GRZ (Great Barrier Island) in the North Island near Auckland. (a) Log₁₀ 10-Hz highpass-filtered envelope function 2 hrs before and after the Kaikōura mainshock. Vertical lines mark the time windows plotted in panels (b–d). (b) Instrument-corrected broadband signals recorded at station GRZ. (c) 10-Hz high-pass-filtered vertical-component seismogram showing the *P* wave of the mainshock and triggered tremor signals during the surface waves. (d) The corresponding spectro-gram (i.e., frequency–time distribution), with stronger amplitudes marked by darker/warmer shadings. (e) A zoom-in plot showing the long-duration tremor-like signals. The color version of this figure is available only in the electronic edition.

accompanying surface waves were located at shallow depth of less than 10 km (ⓐ Figs. S4 and S5). Such shallow sources are consistent with the fact that it was only recorded by stations nearby (Fig. 8) and is likely associated with magmatic processes that feed this active volcano. Volcanic tremor is commonly present in this system (e.g. Hurst, 1992). However, this tremor signal is typically observed between 1 and 3 Hz. Owing to its limited bandwidth, it has been attributed to the

resonance of a single magmatic reservoir (Hurst and Sherburn, 1993). In addition, tremor that peaked at 7 Hz has been observed near the summit of Mt. Ruapehu and interpreted as an excitation of the very shallow hydrothermal system (Sherburn et al., 1999). Because of the overlapping coda waves from the Kaikōura mainshock, we were unable to observe any triggering signals below 10 Hz during the surfacewave windows (E) Fig. S9). However, we note that the triggering wave frequency goes up to 40 Hz and therefore possibly relates to another source. Although localization of the remaining tremor sources in the TVZ is not possible due to data limitations, the most likely source of this activity is near-surface activation of numerous shallow hydrothermal reservoirs. The individuality of plumbing systems of each hydrothermal area makes source depth and mechanism uncertain. However, numerous studies have shown that seismic radiation occurs in the upper few kilometers of these systems, due to phase changes and dynamics of fluids (e.g., Kieffer, 1984; Kedar et al., 1998).

On the other hand, the source around Mt. Ruapehu (E) Fig. S3) and Lake Taupo (E) Fig. S6) generated long-duration signals that were recorded at stations up to ~50 km away (Fig. 8), consistent with their deep-source origin. In both cases, the triggered source is quite different from the previously observed ambient and triggered tremor sources (Fry et al., 2011; Idehara et al., 2014), which were to the east of Mt. Ruapehu and Tongariro (Fig. 8), close to the Manawatu deep slow-slip regions (Wallace and Beavan, 2006). Finally, it is not easy to distinguish whether those instantaneously triggered events were tremor or regular microearthquakes. Because of the short duration (and shallow depth), those tremor-like signals observed near Mt. Tongariro could also be microearthquakes beneath active volcanoes.

On the other hand, stations near Lake Taupo (and south of Mt. Ruapehu) recorded long-duration events with deep origins. Hence, they likely correspond to tremor signals from the deep subduction zone interface (~70 km at these locations) (Williams *et al.*, 2013) or some deep long-period events associated with the volcanic system.

It is worth noting that, whereas abundant triggered seismicity is observed during the large-amplitude surface waves along the TVZ, the corresponding β -value map computed

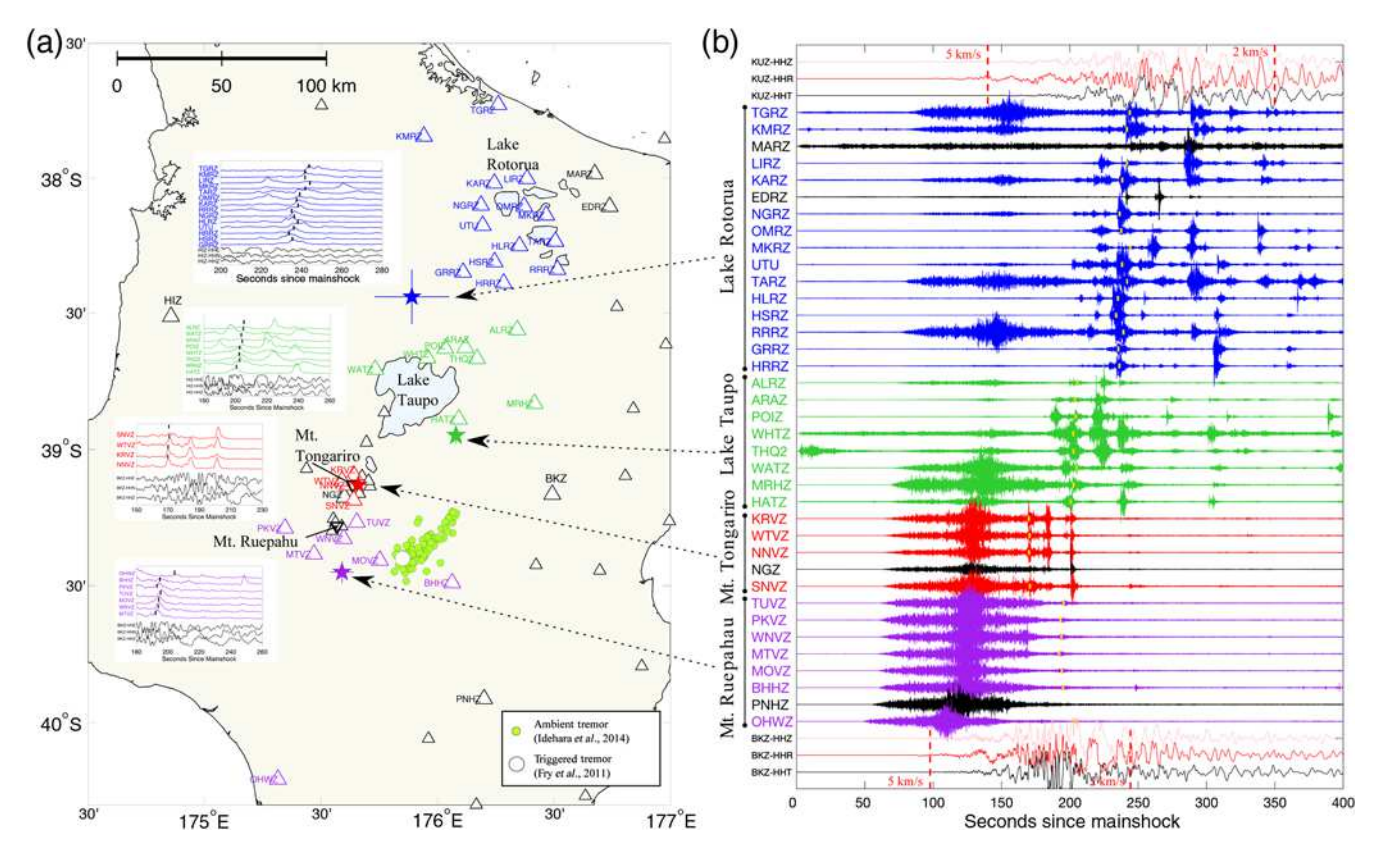


Figure 8. (a) Map showing stations (triangles) around the TVZ that recorded possible triggered seismicity in four regions (stars). Solid and open circles mark the ambient and triggered tremor locations in previous studies. The inset shows the 10–30 Hz band-pass-filtered seismograms used to determine the best-fitting locations (stars). (b) Record section showing all band-pass-filtered seismograms in this region. Arrows link the waveforms to event locations shown in (a). The color version of this figure is available only in the electronic edition.

from one month of microseismicity before and after the mainshock did not show strong rate changes compared with other surrounding regions. In fact, the regions around Mt. Ruapehu and Tongariro showed some rate decrease (Fig. 5). This is likely because of the following reasons. First, the background seismicity rate (i.e., activities before the mainshock) along the TVZ is already relatively high (i.e., Figs. 3a and 5a). Hence, a much higher rate is needed to show a statistically significant rate increase following the mainshock. In addition, because of the extremely high-seismicity rate in the aftershock region, many microearthquakes in the North Island (including the TVZ) were not detected or listed in the current GeoNet catalog, especially right after the mainshock ((E) Fig. S8). This could also explain the clear drop of seismicity in the aftershock zone of the 2016 $M_{\rm w}$ 7.1 Te Araroa earthquake off the East Cape of North Island (Fig. 5). Finally, we note that a uniform magnitude of completeness $M_c = 2.74$ was used in this study. In reality, the magnitude of completeness varies in space and time, especially right after the mainshock (Peng et al., 2007; Hainzl, 2016). To better understand seismicity rate changes in this and other regions of North Island, we need to go beyond the current seismic catalog and detect earthquakes from the continuous waveforms. This is done in a follow-up work (Yao et al., 2017).

In summary, we have shown the widespread activation of tremor and microseismicity following the 2016 $M_{\rm w}$ 7.8 Kai-kōura earthquake. This activation provides evidence of the near-criticality of many faults in the region, as well as the susceptibility of the volcanic or hot spring areas to changes during dynamic stressing. We identified several areas of newly discovered tremor on both North and South Island away from major fault systems, likely associated with regions of hot springs or elevated geothermal gradients (Reyes *et al.*, 2010). The impact of tremor in these regions on future seismic hazard assessment will be addressed in subsequent studies.

Data and Resources

Seismic data and earthquake catalogs analyzed in this study were provided by GeoNet (https://www.geonet.org.nz, last accessed October 2017). The digital fault database can be accessed at http://data.gns.cri.nz/af/ (last accessed September 2017).

Acknowledgments

The authors thank Ian Hamling and Laura Wallace for sharing the digital surface rupture trace of the 2016 Kaikōura mainshock. The article also benefited from useful comments by an anonymous reviewer and John Townend. Z. P. and D. Y. are supported by National Science Foundation Grants EAR-1551022, EAR-1725165, and EAR-1818611. Z. P. acknowledges ad-

ditional support from Georgia Tech College of Science's Faculty Development Grant. K. C. is supported by the Northwestern Institute for Complex Systems (NICO) and the Center for Optimization and Statistical Learning (OSL) at Northwestern University through the Northwestern Data Science Scholars Fellowship. This work is also partially funded by the Royal Society Marsden Fund and GNS core funding.

References

- Aiken, C., J. C. Zimmerman, J., Z. Peng, and J. Walter (2015). Triggered seismic events along the eastern Denali fault in northwest Canada following the 2012 $M_{\rm w}$ 7.8 Haida Gwaii, 2013 $M_{\rm w}$ 7.5 Craig, and two $M_{\rm w} > 8.5$ teleseismic earthquakes, *Bull. Seismol. Soc. Am.* 105, no. 2b, 1165–1177, doi: 10.1785/0120140156.
- Aron, A., and J. L. Hardebeck (2009). Seismicity rate changes along the Central California Coast due to stress changes from the 2003 M 6.5 San Simeon and 2004 M 6.0 Parkfield earthquakes, *Bull. Seismol. Soc. Am.* 99, no. 4, 2280–2292.
- Boodin, M. A., I. E. M. Smith, P. M. Black, and J. L. Mauk (2011). Geochemistry of the early Miocene volcanic succession of Northland, New Zealand, and implications for evolution of subduction in the Southwest Pacific, J. Volcanol. Geoth. Res. 199, 25–37.
- Boodin, M. A., I. E. M. Smith, J. L. Mauk, and P. M. Black (2012). Geochemical and isotopic development of the Coromandel Volcanic Zone, northern New Zealand, since 18 Ma, J. Volcanol. Geoth. Res. 219/220, 15–32.
- Bradley, B. A., H. N. T. Razafindrakoto, and V. Polak (2017). Ground-motion observations from the 14 November 2016 M_w 7.8 Kaikōura, New Zealand, earthquake and insights from broadband simulations, Seismol. Res. Lett. 88, no. 3, 740–756.
- Brodsky, E. E. (2006). Long-range triggered earthquakes that continue after the wave train passes, *Geophys. Res. Lett.* **33**, L15313, doi: 10.1029/2006GL026605.
- Brodsky, E. E., and N. J. van der Elst (2014). The use of dynamic earthquake triggering, *Annu. Rev. Earth Planet. Sci.* **42**, 317–339.
- Chamberlain, C. J., E. Warren-Smith, B. Fry, and J. Townend (2017). Rapid aftershock detection and analysis following the M7.8 Kaikōura earthquake using matched-filter techniques, *Seismol. Res. Lett.* 88, no. 2B, 626
- Chao, K., Z. Peng, Y.-J. Hsu, K. Obara, C. Wu, K.-E. Ching, S. van der Lee, H.-C. Pu, P.-L. Leu, and A. Wech (2017). Temporal variation of tectonic tremor activity in southern Taiwan around the 2010 M_L 6.4 Jiashian earthquake, J. Geophys. Res. 122, doi: 10.1002/ 2016JB013925.
- Cox, S. C., C. D. Menzies, R. Sutherland, P. H. Denys, C. Chamberlain, and D. A. H. Teagle (2015). Changes in hot spring temperature and hydrogeology of the Alpine fault hanging wall, New Zealand, induced by distal South Island earthquakes, *Geofluids* 15, 216–239.
- Enescu, B., K. Shimojo, A. Opris, and Y. Yagi (2016). Remote triggering of seismicity at Japanese volcanoes following the 2016 M7.3 Kumamoto earthquake, *Earth Planets Space*, **68**, no. 1, 165, doi: 10.1186/s40623-016-0539-5.
- Fry, B., S. Bannister, J. Beavan, L. Bland, B. Bradley, S. Cox, J. Cousins, N. Gale, G. Hancox, C. Holden, *et al.* (2010). The $M_{\rm w}$ 7.6 Dusky Sound earthquake of 2009: Preliminary report, *Bull. New Zeal. Soc. Earthq. Eng.* **43**, 24–40.
- Fry, B., K. Chao, S. C. Bannister, Z. Peng, and L. Wallace (2011). Deep tremor in New Zealand triggered by the $2010\,M_{\rm w}$ 8.8 Chile earthquake, *Geophys. Res. Lett.* **38**, L15306, doi: 10.1029/2011GL048319.
- Gomberg, J., P. Bodin, K. Larson, and H. Dragert (2004). The fundamental process of earthquake nucleation by transient deformations revealed by the M 7.9 Denali, Alaska earthquake, *Nature* **427**, 621–624.
- Gomberg, J., P. Reasenberg, P. Bodin, and R. Harris (2001). Earthquake triggering by transient seismic waves following the Landers and Hector Mine, California earthquakes, *Nature* 411, 462–466.

- Gonzalez-Huizar, H., and A. A. Velasco (2011). Dynamic triggering: Stress modeling and a case study, *J. Geophys. Res.* 116, no. B02304, doi: 10.1029/2009JB007000.
- Guilhem, A., Z. Peng, and R. M. Nadeau (2010). High-frequency identification of non-volcanic tremor along the San Andreas fault triggered by regional earthquakes, *Geophys. Res. Lett.* 37, L16309, doi: 10.1029/2010GL044660.
- Hainzl, S. (2016). Rate-dependent incompleteness of earthquake catalogs, Seismol. Res. Lett. 87, no. 2A, 337–344, doi: 10.1785/0220150211.
- Hamling, I. J., S. Hreinsdóttir, K. Clark, J. Elliott, C. Liang, E. Fielding, N. Litchfield, P. Villamor, L. Wallace1, T. J. Wright, et al. (2017). Complex multifault rupture during the 2016 M_w 7.8 Kaikōura earthquake, New Zealand, Science 356, doi: 10.1126/science.aam7194.
- Han, L., Z. Peng, C. W. Johnson, F. F. Pollitz, L. Li, B. Wang, J. Wu, and Q. Li (2017). Shallow microearthquakes near Chongqing, China triggered by the Rayleigh waves of the 2015 M 7.8 Gorkha, Nepal earthquake, Earth Planet. Sci. Lett. 479, 231–240, doi: 10.1016/j.epsl.2017.09.024.
- Heming, R. F. (1980). Petrology and geochemistry of Quaternary Basalts from Northland, New Zealand, J. Volcanol. Geoth. Res. 8, 23–44.
- Hill, D. P. (2012). Dynamic stress, coulomb failure, and remote triggering-corrected, Bull. Seismol. Soc. Am. 102, 2313–2336.
- Hill, D. P., and S. Prejean (2015). Dynamic triggering, in *Treatise on Geophysics*, H. Kanamori (Editor), Second Ed., Vol. 4, Elsevier, Amsterdam, The Netherlands.
- Hurst, A. W. (1992). Stochastic simulation of volcanic tremor from Ruapehu, J. Volcanol. Geoth. Res. 51, 185–198.
- Hurst, A. W., and S. Sherburn (1993). Volcanic tremor at Ruapehu: Characteristics and implications for the resonant source, New Zeal. J. Geol. Geophys. 36, 475–485.
- Idehara, K., S. Yabe, and S. Ide (2014). Regional and global variations in the temporal clustering of tectonic tremor activity, *Earth Planets Space* 66, 66, doi: 10.1186/1880-5981-66-66.
- Kaiser, A., N. Balfour, B. Fry, C. Holden, N. Litchfield, M. Gerstenberger, E. D'Anastasio, N. Horspool, G. McVerry, J. Ristau, et al. (2017). The 2016 Kaikōura, New Zealand, earthquake: Preliminary seismological report, Seismol. Res. Lett. 88, no. 3, 727–739.
- Kedar, S., H. Kanamori, and B. Sturtevant (1998). Bubble collapse as the source of tremor at Old Faithful Geyser, J. Geophys. Res. 103, 24,283– 24,299.
- Kieffer, S. (1984). Seismicity at Old Faithful Geyser: An isolated source of geothermal noise and possible analogue of volcanic seismicity, J. Volcanol. Geoth. Res. 22, 59–95.
- King, G. C. P., and M. Deves (2015). Fault interaction, earthquake stress changes, and the evolution of seismicity, in *Earthquake Seismology, Treatise on Geophysics*, H. Kanamori (Editor), Second Ed., Vol. 4, G. Schubert (Editor-in-Chief), Elsevier, Amsterdam, The Netherlands.
- Li, L., D. Yao, X. Meng, Z. Peng, and B. Wang (2017). Increasing normal-faulting earthquakes in southern Tibet following the 2015 $M_{\rm w}$ 7.8 Gorkha, Nepal earthquake, *Tectonophysics* **714/715**, 62–70, doi: 10.1016/j.tecto.2016.08.008.
- Manga, M., I. Beresnev, E. E. Brodsky, J. E. Elkhoury, D. Elsworth, S. Ingebritsen, D. C. Mays, and C.-Y. Wang (2012). Changes in permeability by transient stresses: Field observations, experiments and mechanisms, *Rev. Geophys.* 50, RG2004, doi: 10.1029/2011RG000382.
- Meng, X., and Z. Peng (2016). Increasing lengths of aftershock zones with depths of moderate-size events on the San Jacinto fault suggests triggering of deep creep, *Geophys. J. Int.* 204, no. 1, 250–261, doi: 10.1093/gji/ggv445.
- Michael, A. J. (2011). Random variability explains apparent global clustering of large earthquakes, *Geophys. Res. Lett.* 38, L21301, doi: 10.1029/2011GL049443.
- Miyazawa, M. (2016). An investigation into the remote triggering of the Oita earthquake by the 2016 $M_{\rm w}$ 7.0 Kumamoto earthquake using full wavefield simulation, *Earth Planets Space* **68**, no. 1, 205, doi: 10.1186/s40623-016-0585-z.

- Nicol, A., N. Khajavi, J. R. Pettinga, C. Fenton, T. Stahl, S. Bannister, K. Pedley, N. Hyland-Brook, T. Bushell, I. Hamling, *et al.* (2018). Preliminary geometry, displacement, and kinematics of fault ruptures in the epicentral region of the 2016 $M_{\rm w}$ 7.8 Kaikōura earthquake, New Zealand, *Bull. Seismol. Soc. Am.* doi: 10.1785/0120170329.
- Obara, K. (2012). New detection of tremor triggered in Hokkaido, northern Japan by the 2004 Sumatra-Andaman earthquake, *Geophys. Res. Lett.* 39, L20305, doi: 10.1029/2012GL053339.
- Opris, A., B. Enescu, Y. Yagi, and J. Zhuang (2017). Triggering and decay characteristics of dynamically activated seismicity in Southwest Japan, *Geophys. J. Int.* 212, 1010–1021, doi: 10.1093/gji/ggx456.
- Peng, Z., and J. Gomberg (2010). An integrated perspective of the continuum between earthquakes and slow-slip phenomena, *Nature Geosci.* **3,** 599–607, doi: 10.1038/ngeo940.
- Peng, Z., L. T. Long, and P. Zhao (2011). The relevance of high-frequency analysis artifacts to remote triggering, *Seismol. Res. Lett.* 82, no. 5, 656–660, doi: 10.1785/gssrl.82.5.654.
- Peng, Z., D. R. Shelly, and W. L. Ellsworth (2015). Delay dynamic triggering of deep tremor along the Parkfield-Cholame section of the San Andreas fault following the 2014 M 6.0 South Napa earthquake, *Geophys. Res. Lett.* 42, 7916–7922, doi: 10.1002/2015GL065277.
- Peng, Z., J. E. Vidale, M. Ishii, and A. Helmstetter (2007). Seismicity rate immediately before and after main shock rupture from high-frequency waveforms in Japan, J. Geophys. Res. 112, no. B03306, doi: 10.1029/ 2006JB004386.
- Pollitz, F. F., R. S. Stein, V. Sevilgen, and R. Bürgmann (2012). The 11 April 2012 east Indian Ocean earthquake triggered large aftershocks worldwide, *Nature* 490, 250–255, doi: 10.1038/nature11504.
- Prejean, S. G., D. P. Hill, E. E. Brodsky, S. E. Hough, M. J. S. Johnston, S. D. Malone, D. H. Oppenheimer, A. M. Pitt, and K. B. Richards-Dinger (2004). Remotely triggered seismicity on the United States west coast following the $M_{\rm w}$ 7.9 Denali fault earthquake, *Bull. Seismol. Soc. Am.* **94**, S348–S359.
- Reyes, A. G., B. W. Christenson, and K. Faure (2010). Sources of solutes and heat in low-enthalpy mineral waters and their relation to tectonic setting, New Zealand, J. Volcanol. Geoth. Res. 192, 117–141.
- Sherburn, S., C. J. Bryan, A. W. Hurst, J. H. Latter, and B. J. Scott (1999). Seismicity of Ruapehu volcano, New Zealand, 1971–1996: A review, J. Volcanol. Geoth. Res. 88, 255–278.
- Tape, C., M. West, V. Silwal, and N. Ruppert (2013). Earthquake nucleation and triggering on an optimally oriented fault, *Earth Planet. Sci. Lett.* 363, 231–241.
- Wallace, L. M, and J. Beavan (2006). A large slow slip event on the central Hikurangi subduction interface beneath the Manawatu region, North Island, New Zealand, Geophys. Res. Lett. 33, L11301, doi: 10.1029/2006GL026009.
- Wallace, L. M., Y. Kaneko, N. Bartlow, S. Hreinsdottir, I. Hamling, Z. Peng, E. D'Anastasio, and B. Fry (2017). Large-scale dynamic triggering of a shallow slow slip event enhanced by low-velocity sediments, *Nature Geosci.* 10, 765–770, doi: 10.1038/ngeo3021.
- Wang, C.-Y., and M. Manga (2010). Hydrologic responses to earthquakes— A general metric, Geofluids 10, 206–216.
- Warren-Smith, E., C. J. Chamberlain, S. Lamb, and J. Townend (2017). High-precision analysis of an aftershock sequence using matched filter detection: The May 4 2015 M_L 6 Wanaka earthquake, Southern Alps, New Zealand, Seismol. Res. Lett. 88, doi: 10.1785/0220170016.

- Wech, A. G., C. M. Boese, T. A. Stern, and J. Townend (2012). Tectonic tremor and deep slow slip on the Alpine fault, *Geophys. Res. Lett.* **39**, L10303, doi: 10.1029/2012GL051751.
- Wen, Y.-Y., K.-F. Ma, and B. Fry (2018). Multiple-fault, slow rupture of the 2016 $M_{\rm w}$ 7.8 Kaikōura, New Zealand, earthquake: Complementary insights from teleseismic and geodetic data, *Bull. Seismol. Soc. Am.* doi: 10.1785/0120170285.
- Williams, C. A., A. Eberhart-Phillips, S. Bannister, D. H. N. Barker, S. Henrys, M. Reyners, and R. Sutherland (2013). Revised interface geometry for the Hikurangi subduction zone, New Zealand, *Seismol. Res. Lett.* 84, no. 6, 1066–1073, doi: 10.1785/0220130035.
- Wiemer, S. (2001). A software package to analyze seismicity: ZMAP, Seismol. Res. Lett. 72, 373–382.
- Wiemer, S., and M. Wyss (2000). Minimum magnitude of completeness in earthquake catalogs: Examples from Alaska, the western United States, and Japan, Bull. Seismol. Soc. Am. 90, no. 4, 859–869.
- Woessner, J., and S. Wiemer (2005). Assessing the quality of earthquake catalogues: Estimating the magnitude of completeness and its uncertainty, Bull. Seismol. Soc. Am. 95, no. 2, 684–698, doi: 10.1785/0120040007.
- Yao, D., Z. Peng, B. Fry, L. Wallace, Y. Kaneko, and X. Meng (2017). Dynamically triggering of microseismicity in the North Island of New Zealand following the $M_{\rm w}$ 7.8 Kaikōura earthquake, presented at the 2017 Fall Meeting, AGU, New Orleans, Louisiana, 11–15 December, Abstract S23B–0799.

School of Earth and Atmospheric Sciences Georgia Institute of Technology 311 Ferst Drive Atlanta, Georgia 30338 zpeng@gatech.edu (Z.P., D.Y.)

GNS Sciences 1 Fairway Drive, Avalon 5010 PO Box 30-368 Lower Hutt 5040 New Zealand (B.F., A.J.)

Department of Earth and Planetary Sciences 2145 Sheridan Road, Room F374 Evanston, Illinois 60208 (K.C.)

Department of Earth Sciences University of Southern California 3651 Trousdale Parkway Los Angeles, California 90089 (X.M.)

> Manuscript received 31 October 2017; Published Online 22 May 2018